ELSEVIER

Biophysical Chemistry 125 (2007) 191–200

Biophysical Chemistry

http://www.elsevier.com/locate/biophyschem

The study of helical distortions due to environmental changes: Choice of parameters

R. Sreekanth, S.S. Rajan *

Deparment of Crystallography and Biophysics, University of Madras, Chennai, India

Received 18 May 2006; received in revised form 28 July 2006; accepted 29 July 2006
Available online 17 August 2006

Abstract

Parameters like interhelical angles, helical parameters, levels of distortions, etc., have been analysed to test their sensitivity to environmental changes using a method developed in this laboratory. This analysis was done on protein structures solved under different environmental conditions like temperature and pH, and ligand binding. The study reveals that the helical parameters are not sensitive enough to study the effect of environmental changes on protein helices. On the other hand the helical distortions as well as changes in the interhelical angles are more sensitive to these changes. The study also provides with additional information like the origin of distortions in a helix when a ligand binds to a protein, bending in helical axis, identification and extent of domain movements, etc.

Keywords: Helical parameters; η_{ij} maps; Helical distortions; Interhelical angles; Environmental changes

1. Introduction

A large number of protein structures have been solved at high resolution using X-ray crystallographic and NMR techniques and the data are available in the Protein Data Bank [1]. It is important to analyse this vast data to extract information regarding the properties of these proteins and if possible correlate with their function. One such analysis pertains to the study of distortions and bends in α-helices, relative orientations of helices, helical parameters, etc. In most protein structures the helices are distorted to different levels and in a few cases the helical axes are curved rather than straight. This knowledge about the details of α-helical structures and their distortions are essential to completely understand the protein structure, folding and function [2–4]. Different methods are available in the literature for calculating the helical axis and helical parameters [5–7]; however these methods do not deal with the distortions in helices. In our analysis, the method proposed by Srinivasan and co-workers [8–12] was used to characterize the helical regions like bends, the levels of distortions, etc., and to calculate the helical parameters and inter helical angles. As a first step, the method used was validated against other available algorithms [5,6].

It is also well known that when a protein is subjected to different conditions like pH, temperature or when it interacts with a ligand, distortions/changes occur in different parts of the protein which need not necessarily be only at the binding site. Acid-induced folding [13] and thermal expansion of proteins [14,15] emphasize the importance of the environment on protein structures. Reports on acid/thermal denaturation on barnase [16], ribonuclease S [17] and apomyoglobin [18] have shown unfolding of N-terminal region of helices, increase in helical disorder and overall helical unfolding highlighting the role of alpha helices on protein stability against pH and temperature. Further UV-CD studies on alpha crystalline indicate an increase in the alpha helical content as temperature is increased and these structural alterations are reported to be functionally important [19]. An extensive analysis on the alpha helical properties that influence the thermal stability of proteins is also available in the literature [20,21].

It is of interest to find out the parameters that are suitable to detect these changes. Although several regions of the structures other than the helices may also get affected, we confined our

* Corresponding author. Fax: +91 44 22352494.
E-mail address: ssrsai@hotmail.com (S.S. Rajan).

0301-4622/$ - see front matter © 2006 Elsevier B.V. All rights reserved.
doi:10.1016/j.bpc.2006.07.014

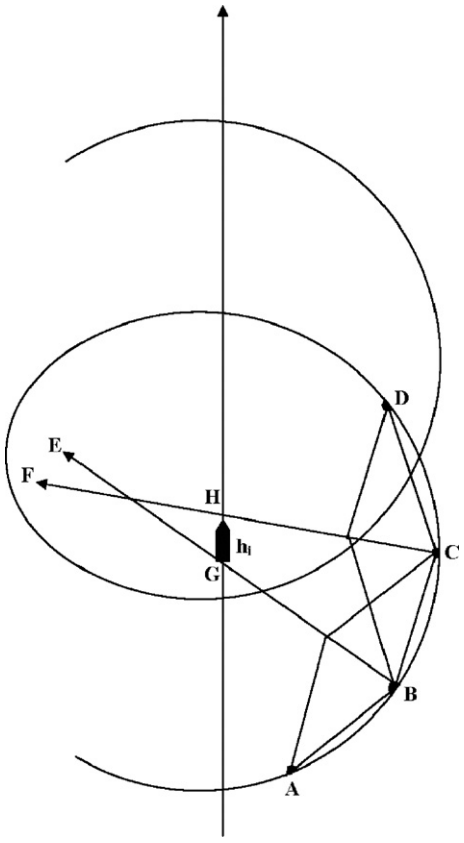

Fig. 1. Schematic diagram to illustrate the construction of the helical axis. A, B, C and D are the positions of the four consecutive C^{α} atoms. BE and CF are the bisectors of angles ABC and BCD, respectively. GH is the skew line for BE and CF which represents the h_i vector. The angle formed between h_i and h_j ($j=i, n$, where n=total no. of h_i vectors in the helix) vectors is the η_{ij} angle.

study only to the helical regions due to the ease with which the changes in this region can be quantified.

In this context, we have analysed protein structures solved under different pH, humidity conditions and temperatures. In addition, protein–ligand complexation has also been taken up for analysis. Changes in the values of helical parameters, comparison of η_{ij} maps (described in Materials and methods) of native and modified proteins, the interhelical angles and standard deviations in η_{ij} values were studied for each set of proteins. The analysis using these parameters has been effective in bringing out various structural changes in proteins solved under different environments.

Table 1
The l, m, n values (directional cosines) of the A-helix (4–17) in myoglobin molecule solved at 1 Å obtained using the present method is in good agreement with other methods

	l	m	n
RADIL (present method)	0.966	0.257	−0.028
AQVIST	0.954	0.296	−0.037
EIGENFIT	0.959	0.278	−0.060
HELANAL	0.948	0.247	−0.024
KAHN	0.960	0.275	−0.045
PARLSQ	0.959	0.277	−0.059
ROFIT	0.965	0.261	−0.036
SIMPLEFIT	0.942	0.335	−0.016

Table 2
Differences in interhelical angles (deg) in lysozyme structure between 95K and 295K showing a change in interhelical angles as the differences in temperature increases

Structures ↓	Angle between helices →					
	H1–H2	H1–H3	H1–H4	H2–H3	H2–H4	H3–H4
95K–120K	–1	0	0	0	0	–1
95K–180K	0	0	0	0	0	
95K–250K	1	0	4	0	–4	3
95K–280K	4	1	2	0	–6	4
95K–295K	2	0	5	1	–6	4

2. Materials and methods

2.1. The database

PDB [1] (http://www.rcsb.org/pdb/), OCA (http://bip.weizmann.ac.il/oca) and PDBLITE (http://pdblite.org) databases provided the coordinates of protein structures solved under different humidity, pH and temperature conditions. The protein–ligand complex structures were plenty as compared to other categories. Resolutions of the structures under each category were comparable. As the analysis was confined only to the helical regions, the protein structures were chosen such that they contain a large number of long helices. The starting and ending residues of helices were taken as reported in the PDB entry. The database used for the analysis is given as Supplementary material.

2.2. The algorithm and tool

The analysis was carried out using the methods and programs developed [8–12] from this laboratory. In this method, a vector h_i is defined using the positional coordinates of four consecutive C^{α} atoms (Fig. 1). The parameter η_{ij}, which represents the angle between the vectors h_i and h_j, gives the relative orientations of the local axes between ith and jth vectors. For an ideal helix, the

Table 3
Helical parameters and the standard deviations in brackets for troponin C solved at 280 K and 303 K

Helix no. and starting and ending residues		Radius (Å)	Rise/residue (Å)	Rotation/residue (deg)
Helix 1 (2–11)	280 K	2.2 (5)	1.7 (6)	98 (9)
	303 K	2.1 (4)	1.7 (5)	106 (14)
Helix 2 (13–28)	280 K	2.4 (6)	1.5 (7)	95 (23)
	303 K	2.3 (3)	1.5 (4)	100 (8)
Helix 3 (41–49)	280 K	2.3 (1)	1.5 (2)	100 (5)
	303 K	2.4 (2)	1.5 (2)	96 (7)
Helix 4 (53–65)	280 K	2.4 (3)	1.5 (3)	96 (10)
	303 K	2.4 (2)	1.5 (3)	97 (9)
Helix 5 (74–86)	280 K	2.3 (5)	1.5 (5)	101 (21)
	303 K	2.5 (1)	1.5 (9)	102 (41)

The values are comparable in these two temperatures.

Table 4
Differences in interhelical angles (deg) as observed in troponin C structures solved at 280 K and 303 K, indicating the change in the orientation of the helices due to an increase in temperature

1	0				
2	–11	0			
3	35	9	0		
4	–18	18	–11	0	
5	19	–5	–20	–7	0
	1	2	3	4	5

Helix no. ⟶

The helix numbers are given along side.

η_{ij} values should be zero; however for an observed helix the values of η_{ij} define the levels of distortion in the helices. The η_{ij} values were divided into three regions and are marked as A (0°–6°), B (6°–11°) and C (>11°) as defined in the original paper [11,12] to represent least, medium and high levels of distortions in helices. The deviation from the ideal helix can be estimated by the standard deviation in η_{ij}, given by

$$\sigma(\eta_{ij}) = \sqrt{(\sum \eta_{ij}^2/n)}$$

As the resolutions of the protein structures analysed in this paper are between 1.5 and 2.5 Å, an error analysis [11,12] in η_{ij} showed that a five degree difference can be considered to be significant. This method enables one to calculate the best axes for the helices and hence, the best helical parameters. The relative orientations of different helices can be calculated once the axes of these helices are known. Successive h_i vectors represent the course of movement of the protein chain. This representation of h_i vectors is designated as axoidal plot.

2.3. Comparison of other algorithms used for defining helical axis

Several algorithms [5] like AQVIST, EIGENFIT, KAHN, PARLSQ, ROFIT, SIMPLEFIT, HELANAL [6], HA [7] are available in the literature for calculating the average helical axis. The present method used was initially checked and validated with the existing techniques for defining the helical axis. The *l*, *m*, *n* (direction cosines) values (Table 1) calculated using the present method for the A-helix of myoglobin (*PDB1A6M*) solved at 1 Å resolution shows a good agreement with other known methods [5,6]. In addition, the interhelical angles calculated by the present method were found to be in good agreement with those obtained from INTERHLX [22,23] a program, used for calculating the interhelical angles.

3. Results and discussion

3.1. Effect of temperature

Lysozyme has been the target in the study of structural behaviour of proteins under varying conditions such as

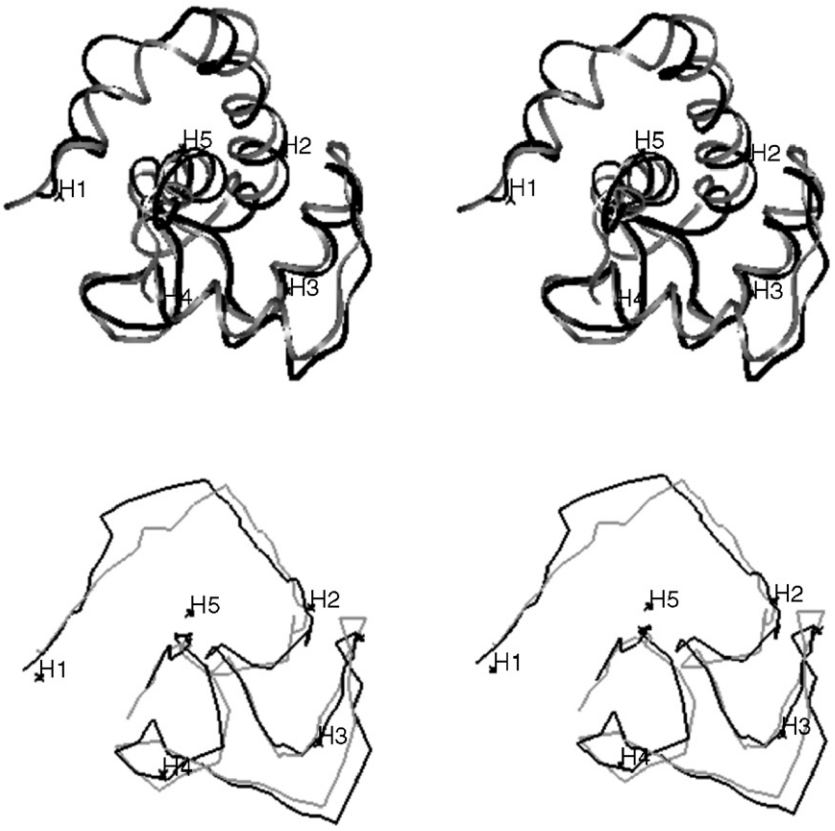

Fig. 2. Stereo diagrams of superposition of the ribbon (top) and axoidal (bottom) representation of troponin C solved at 280 K (grey) and 303 K (black). The helical movements are brought with better clarity in the axoidal plot.

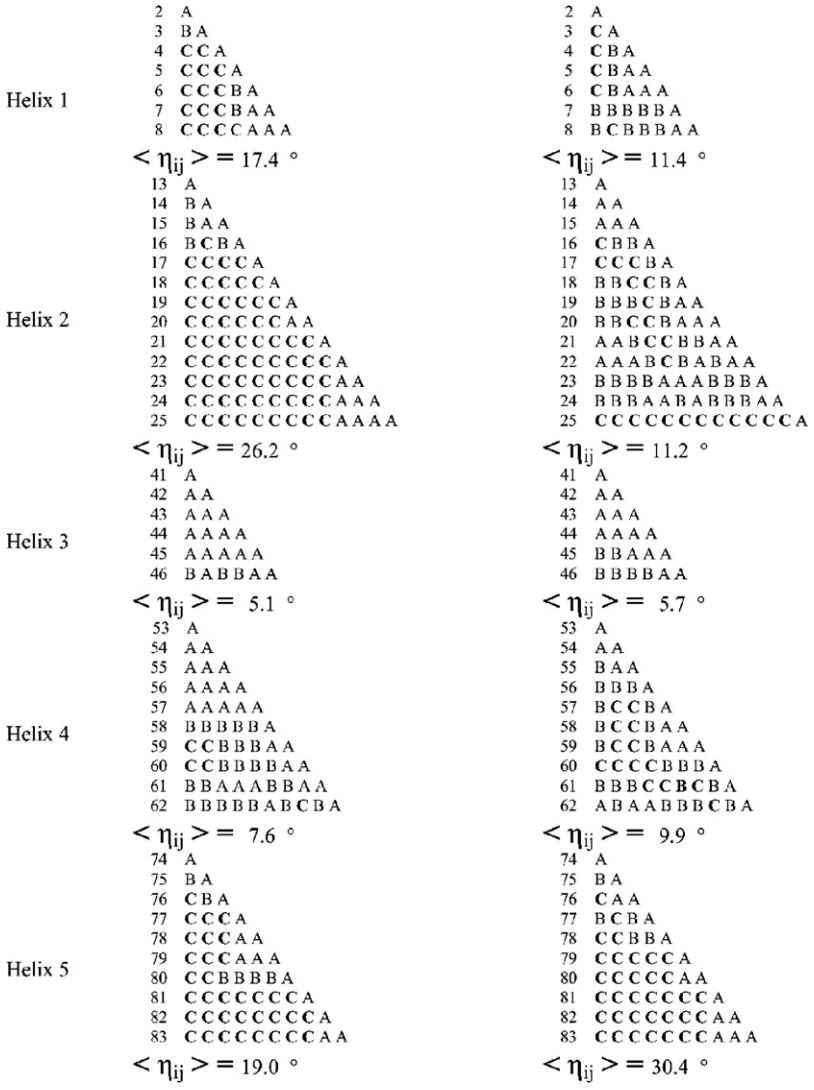

Fig. 3. η_{ij} maps for the five helices of troponin C solved at 280 K (left) and 303 K (right) along with $\sigma(\eta_{ij})$ values illustrating the levels of distortions as the temperature is varied. A, B and C (in bold) in these maps indicate the values of η_{ij} angles falling in the range of 0°–6°, 6°–11° and >11°, respectively. From the figure one can observe that for helices 1 and 2 the levels of distortion are reduced as the temperature is increased, while helices 3 and 4 are not significantly disturbed and in helix 5 the levels of distortion increase. The residue numbers are given alongside.

temperature, pressure, humidity, mutations, etc. The structure of Lysozyme which has been solved at six different temperatures [24] viz., 95 K (*PDB1LSF*), 120 K (*PDB1LSA*), 180 K (*PDB1LSB*), 250 K (*PDB1LSC*), 280 K (*PDB1LSD*) and 295 K (*PDB1LSE*), using X-ray crystallography, exhibits thermal expansion as a result of local atomic packing and secondary structural elements [24]. Here the individual helices are not distorted significantly as the temperature is varied; however the structural changes, on variation of temperature, are reflected in the differences in interhelical angles (Table 2). Although the expansion of the protein has been discussed in the original paper the helical analysis done by the present method helps in quantifying the movement.

Similar results have been obtained for troponin C which was solved at two different temperatures, viz., 280 K (*PDB1R6P*) and 303 K (*PDB1R2U*), using NMR [25]. The helical parameters (r,θ,h) calculated for the helices in the two structures at two different temperatures (Table 3) reveal that they are not sensitive to environmental changes. It has been reported that there is an expansion of the protein at higher temperature [25]. The structural changes observed through large differences in the interhelical angles of the two structures (Table 4), as the

Table 5
Differences in interhelical angles (deg) for phosphoribosylglycinamide formyltransferase point out that helices 4 to 7 have orientational changes (in bold) for a change of pH from 8.5 to 4.2

1	0						
2	1	0					
3	5	2	0				
4	**6**	**5**	**5**	**0**			
5	**–2**	**–1**	**9**	**2**	**0**		
6	**6**	**9**	**–9**	**10**	**9**	**0**	
7	**–7**	**–9**	**12**	**–4**	**–4**	**4**	**0**
	1	2	3	**4**	**5**	**6**	**7**

Helix no. →

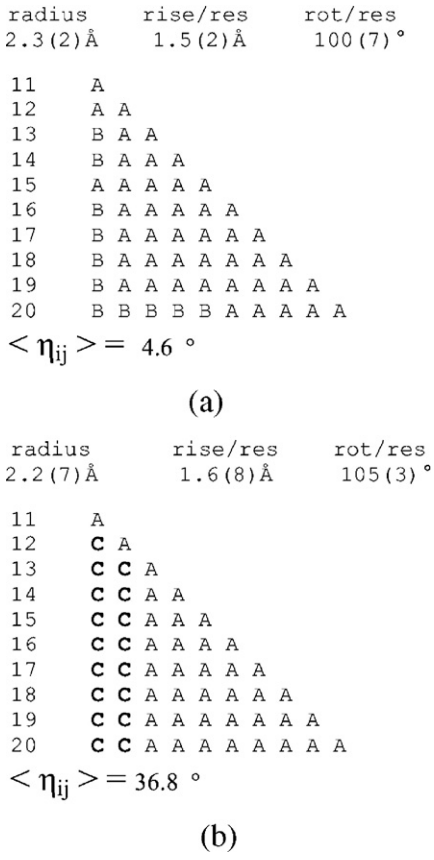

Fig. 4. η_{ij} map for helix 1 (11–23) of phosphoribosylglycinamide formyltransferase at pH 8.5 (a) and pH 4.2 (b) along with the helical parameters and standard deviation showing a N-terminal distortion, with a large distribution of Cs (in bold), being introduced at acidic pH.

temperature is increased, are significant in this structure compared to lysozyme. The axoidal plot calculated (Fig. 2) using the local helical axis also reveals this fact. In addition to confirming the earlier observation, the method gives an estimate of the levels of distortions in helices at these two temperatures. It is seen from the η_{ij} maps (Fig. 3) that the distortions in helices 1 and 2 are reduced as seen from the reduction in the number of *C*s as the temperature increases from 280 to 303 K while in helix 5 the level of distortion increases. The changes in the levels of distortions in helices 3 and 4 are not significant. These are also reflected in the standard deviations in η_{ij}.

3.2. Effect of pH

The protein phosphoribosylglycinamide formyltransferase, solved using crystallography, at two distinct pH viz., 8.5 (*PDB1MEJ*) and 4.2 (*PDB1MEO*), contains seven helices [26]. There is no change either in the helical parameters or in helical distortions excepting for the helices 1 (11–23) and 7 (161–186) as seen from the η_{ij} maps. However the changes in the interhelical angles (Table 5) suggest that helices 4 to 7 have orientational changes corresponding to the change of pH from 8.5 to 4.2. An N-terminal distortion is introduced while going from pH 8.5 to 4.2 in the first helix (Fig. 4). This also indicates that the denaturation of helix 1 (11–24) starts from the N terminal end. The η_{ij} map for the helix 7 at pH 8.5 (Fig. 5) shows that this helix consists of three distinct helical regions. The standard deviation in η_{ij} values for these three regions changes from 3.9 to 4.1 (helix 7A), 2.0 to 7.1 (helix 7B) and 7.1 to 7.4 (helix 7C) from pH 8.5 to 4.2, respectively, indicating that the middle portion of this helix (helix 7B) is

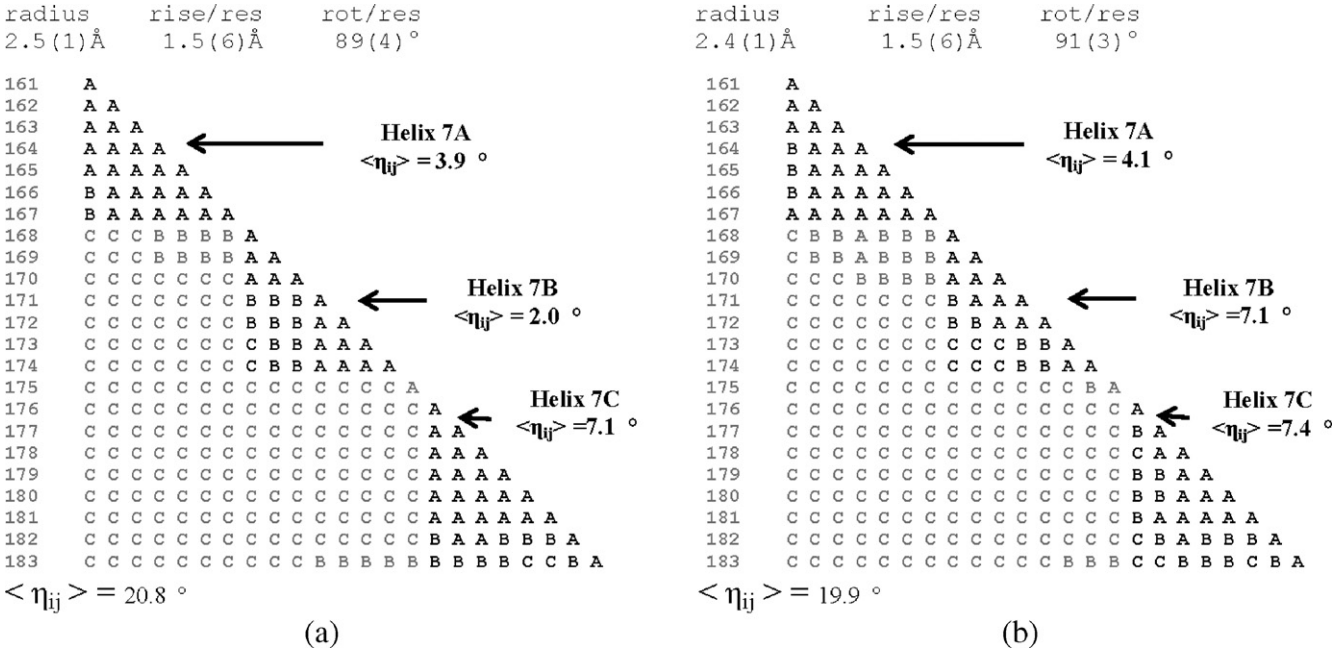

Fig. 5. η_{ij} map for helix 7 (161–186) of phosphoribosylglycinamide formyltransferase at pH 8.5 (a) and pH 4.2 (b) along with the helical parameters and standard deviations. The helix consists of three good regions (shown in black) viz., 7A (161–170), 7B (171–177), 7C (178–186) with the middle region undergoing distortion as the pH is lowered, evident from the $\sigma(\eta_{ij})$ given alongside.

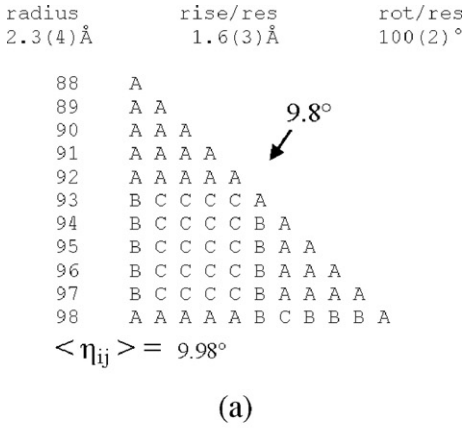

Fig. 6. η_{ij} map for helix 4 (88–101) of lysozyme at 17.6% (a), 16.9% (b) and 9.4% (c) solvent content along with their helical parameters, showing an increase in the degree of bending indicated by the $\sigma(\eta_{ij})$ values, as the solvent content is lowered.

more distorted (Fig. 5) than the other two. When pH is changed from 8.5 to 4.2 the regions at N- and C-terminal ends of the helix remain intact while the distortions are introduced in the central region of the helix. These facts are brought out for the first time by the present method.

3.3. Effect of humidity

In a similar way an analysis was made on the protein lysozyme from *Gallus gallus* solved, using X-ray crystallography, at three low humidity forms at pH 4.2, viz., 17.6% (*PDB1XEI*), 16.9% (*PDB1XEJ*) and 9.4% (*PDB1XEK*) solvent content levels [27]. The η_{ij} maps indicate the regions of distortions as the humidity is lowered (Figs. 6 and 7). The helices 1 (5–15) and 2 (25–36) show N- and C-terminal distortions, respectively (not shown). A bend of 9.8° seen in helix 4 (88–101) at 17.6% solvent content has increased to 18.0° at 9.4% solvent content (Fig. 6). The levels of distortions also increase correspondingly. In helix 5 an ordering is observed when the solvent content is decreased (Fig. 7).

3.4. Effect of ligand binding

The method was also applied to study domain movements on ligation. Calmodulin (*PDB1CLL*) from *Homo sapiens* when complexed with a small molecule, trifluoperazine, (*PDB1CTR*) undergoes large domain movements [28] (Fig. 8). The complexed form is reported to be in CLOSED state and the native in OPEN state. The changes in interhelical angles between the complexed and native forms are given in Table 6. The domain movements can well be visualized from the large differences in the interhelical angles before and after the binding of the ligand. It can be

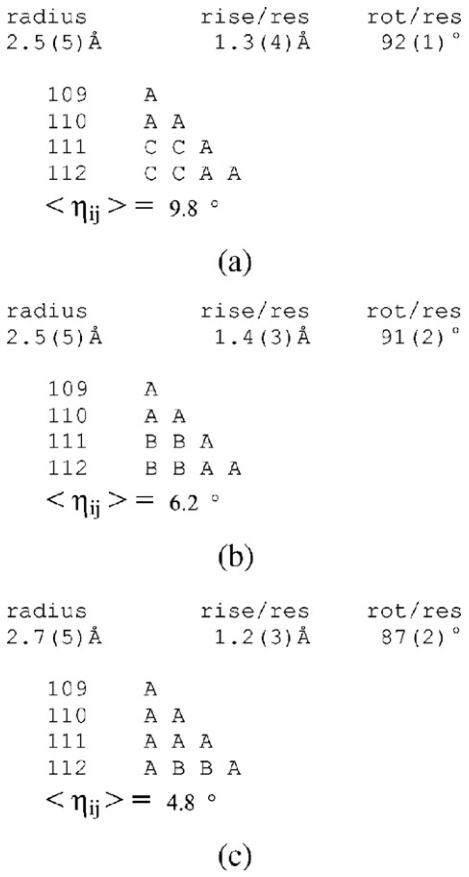

Fig. 7. η_{ij} map for helix 5 (109–115) of lysozyme, at 17.6% (a), 16.9% (b) and 9.4% (c) solvent content, showing that this helix becomes ordered as the solvent content is lowered.

seen from Table 6 that the intradomain movements (angles formed by helices within individual domains) are minimal. A similar observation was made in maltrodextrin binding protein (*PDB1OMP*) bound with maltose (*PDB1ANF*) [29] and also in few other proteins possessing two or more domains.

A ligand-induced bending was observed in cytidine monophosphate kinase (*PDB1CKE*) when complexed with CDP (*PDB2CMK*) [30]. The bending angle in helix 4 (94–105) changes from 9.1° to 19.1° upon binding of the ligand. This has been identified from the η_{ij} maps (Fig. 9) and represented through the axoidal plot (Fig. 10).

In the case of lytic transglycosylase from Bacteriophage Lambda solved using crystallography it has been reported that the sixth helix (135–149) undergoes transition upon ligand binding (*PDB1AM7* is the unbound form and *PDB1D9U* the ligand complexed form) [31]. The $\sigma(\eta_{ij})$ values changes from 11.9° to 74.9° showing that the distortions are introduced on binding of the ligand (Fig. 11). An analysis of the η_{ij} maps (Fig. 11) reveal that this is due to the large N-terminal distortions introduced upon binding which is also reflected on the helical parameters. Thus the present method can also give information on helical transition.

Finally an attempt was made to evaluate the suitability of this method to yield information regarding structure function relationship of proteins. The protein retinoic acid receptor gamma (*PDB2LBD*) [32] from *H. sapiens* has been solved with two ligands, one being active (*PDB1EXA*) and the other inactive (*PDB1EXX*) [33]. The present study indicates that N-terminal distortions are introduced in helix 4 when the active ligand binds whereas for inactive ligand this helix is undistorted (Fig. 12). Similarly helix 1 undergoes high distortions upon binding of an active ligand (Fig. 13) and

Table 6
The differences in interhelical angles (deg) of calmodulin after and before ligand binding, showing large interdomain movement (in bold) between the N-terminal (indicated by helix numbers 1–4) and C-terminal (indicated by helix numbers 5–8) domains compared to the minimal intradomain movement (in grey)

N	1	0							
N	2	–9	0						
N	3	8	0	0					
N	4	–13	–1	3	0				
C	5	**20**	**–38**	**–13**	**–79**	0			
C	6	**107**	**–45**	**–84**	**–69**	4	0		
C	7	**–76**	**44**	**55**	**108**	–5	1	0	
C	8	**40**	**–32**	**–30**	**–30**	–1	–5	8	0
		1	2	3	4	5	6	7	8
		N	N	N	N	C	C	C	C
Helix no.		→							

The large distribution of negative angles within the box indicates that there is a domain closure after ligand binding.

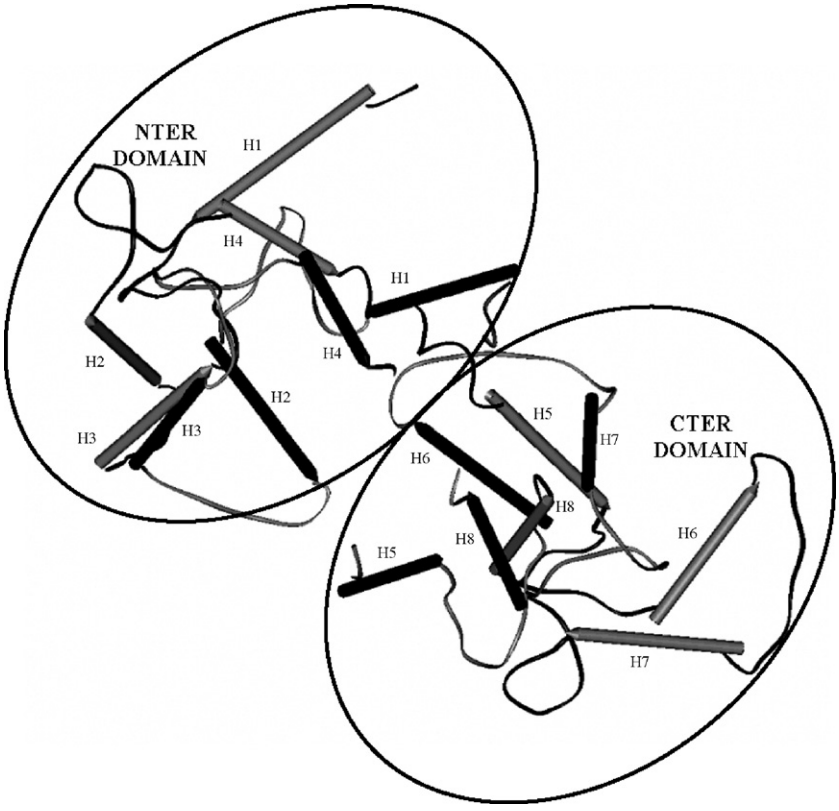

Fig. 8. Cartoon representation of calmodulin in the OPEN state, before binding (grey helices) and CLOSED state, after binding (dark helices) with the ligand. The N-terminal domain consists of helices 1–4 and C-terminal consists of 5–8.

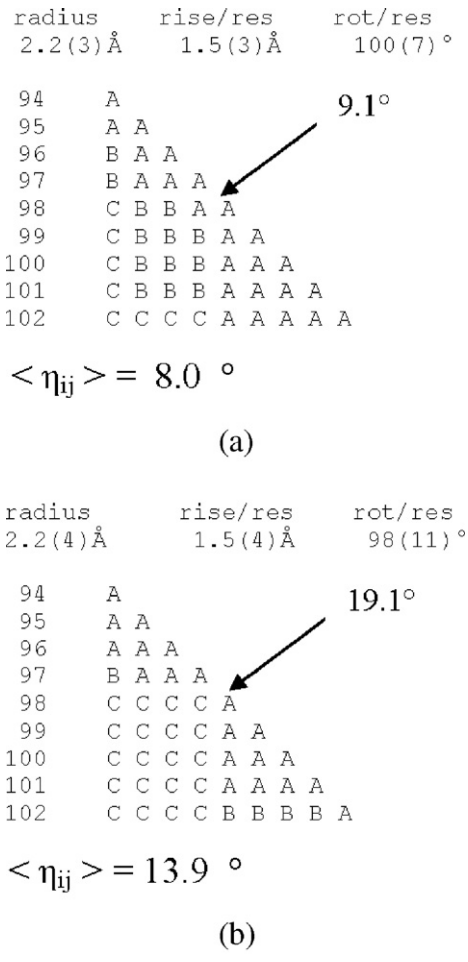

Fig. 9. η_{ij} map for helix 4 (94–105) of cytidine monophosphate kinase before (a) and after (b) complexation. Due to binding of ligand via a water molecule with residue 97, an increase in the bending angle is being observed in this helix near that residue.

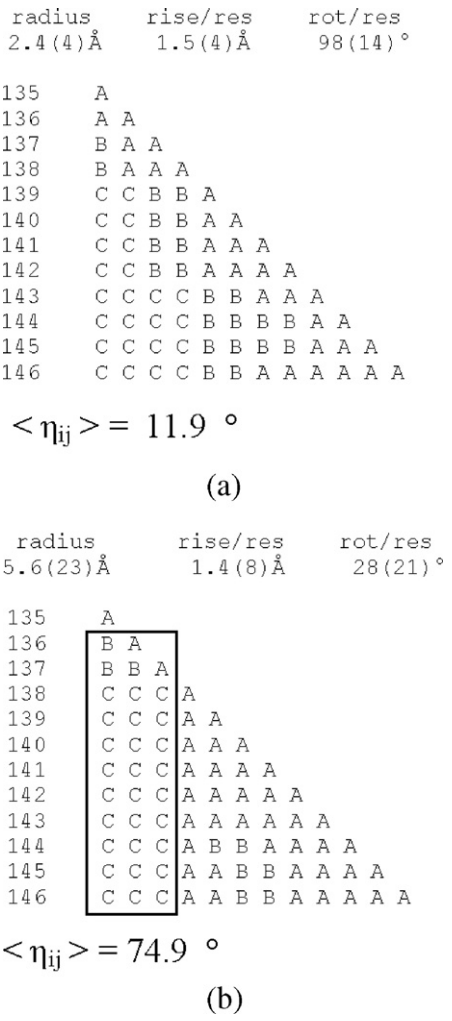

Fig. 11. η_{ij} map for helix 6 (135–149) of lytic transglycosylase before (a) and after (b) complexation, indicating the transition from helicity (within the box) extensively supported by the helical parameters and the $\sigma(\eta_{ij})$ value.

minimum change for the inactive ligand binding. The middle portion of the helix is more distorted on active ligand binding while the helical stretch on either end remains intact. Thus the present analysis has revealed new information in addition to confirming the earlier observations.

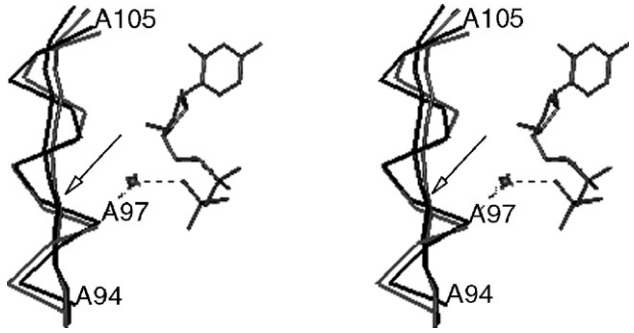

Fig. 10. Stereo picture of helix 4 of cytidine monophosphate kinase before (black) and after (grey) complexation. The axoidal representation clearly indicates the bending near residue 97 due the binding of the ligand (in grey) via a water molecule (in grey) with residue 97.

4. Conclusions

A range of parameters calculated using the present algorithm has been used to bring out various structural features of proteins solved under different environments. The analysis has not only thrown light on local helical distortions but also on the whole protein architecture as such. One of the derived parameters namely the difference in interhelical angles has been used to quantify the extent and mode of domain movement. This parameter can be used to detect the compression or expansion of proteins as a result of change in temperature. The η_{ij} map is another tool to effectively identify bends in helical axis and N- and C-terminal distortions. Further, transitions from helicity can be identified from η_{ij} maps which is also reflected in the deviations from ideal helical parameters and their standard deviations. This study indicates that not only the helices near the ligand binding site are affected but also the ones away from it. Therefore, structure analysis and comparison should consider the protein as a whole and not the binding region alone. Introduction of bends, change in bending regions or amount

```
radius      rise/res     rot/res
2.3(2)Å      1.5(2)Å      100(8)°

   266     A
   267     A A
   268     B B A
   269     B B B A
   270     A B B A A
   271     A B B B A A
   272     A B C B A A A
   273     B B C C C B B A
   274     B A B C C B C B A
   275     B A A B B B C C A A
```

$< \eta_{ij} > =$ 9.1 °

(a)

```
radius      rise/res     rot/res
2.3(4)Å      1.6(8)Å      100(2)°

   266     A
   267     C A
   268     C C A
   269     C C B A
   270     C C B A A
   271     C C B A A A
   272     C C B B A A A
   273     C C B B B A A A
   274     C C A B A A B A A
   275     C C A B B A B A A A
```

$< \eta_{ij} > =$ 21.2 °

(b)

```
radius      rise/res     rot/res
2.3(2)Å      1.5(2)Å      100(8)°

   266     A
   267     A A
   268     A A A
   269     A A A A
   270     A A A A A
   271     B B B A A A
   272     B B C B B B A
   273     A B B B B B A A
   274     A A A A A B B B A
   275     A A A A A A B B A A
```

$< \eta_{ij} > =$ 6.2 °

(c)

Fig. 12. η_{ij} map for helix 4 (266–278) of retinoic acid receptor gamma: (a) native state, (b) binding of an active ligand introduces N-terminal distortion and (c) binding of an inactive ligand leaves the η_{ij} map undisturbed.

of change in bending angle can be quantified from η_{ij} values and their standard deviations for each helix. Helices may undergo small distortions which may not be reflected in the conventional helical parameters. However, even small distortions in the helices can be identified using the η_{ij} map. Thus the present method is useful in characterizing and quantifying helical distortions and other changes due to environmental conditions. The present method can well be adopted for studying small helical distortions, changes in the orientations

```
radius      rise/res     rot/res
2.3(2)Å      1.5(2)Å      98(8)°

   183     A
   184     A A
   185     B B A
   186     B B A A
   187     A B B A A
   188     A A B B A A
   189     A A B B A A A
   190     A A B B B A A A
   191     A A B B B A B A A
   192     A A A A A A B B A A
   193     A B B A A A A B B A A
   194     A A B B A A A A A A A A
   195     A A B B B A A A A A A A A
   196     A A A B B A A A A A A A A A
   197     A A B B B A B A A A B B A A A
```

$< \eta_{ij} > =$ 5.5 °

(a)

```
radius      rise/res     rot/res
2.3(6)Å      1.6(6)Å      99(3)°

   183     A
   184     A A
   185     A A A
   186     A A A A
   187     A A A A A
   188     C C C C C A
   189     C C C C C C A
   190     C C C C C C C A
   191     C C C C C C C C A
   192     A A A A A C C C C A
   193     A A A A A B C C C B A
   194     B B B B A C C C C B A A
   195     B B B B A C C C C B B A A
   196     B A B B A C C C C B B A A A
   197     B B B B B C C C C B B B A A A
```

$< \eta_{ij} > =$ 26.8 °

(b)

```
radius      rise/res     rot/res
2.3(1)Å      1.5(2)Å      98(5)°

   183     A
   184     A A
   185     A A A
   186     A A A A
   187     A A A A A
   188     A A A A A A
   189     A A B A A A A
   190     B B B B B A A A
   191     B A B B B A B A A
   192     A A A A A A B B A A
   193     A A A A A A A B B A A
   194     A B B B A A A A A B A A
   195     B B B B B B B A A B B A A
   196     A A A B B A B A A A B B A A
   197     B A A B B B B B A A B B A A A
```

$< \eta_{ij} > =$ 5.2 °

(c)

Fig. 13. η_{ij} map for helix 1 (183–200) of retinoic acid receptor gamma before binding (a) and after binding with the active ligand (b) and inactive ligand (c), indicating that this helix is distorted as the active ligand binds (the Cs are shown in bold) and the native state is undisturbed when the inactive ligand binds.

of helices, helical parameters, thermal expansion, helix coil transition, etc.

Acknowledgements

We thank Prof. Vasantha Pattabhi for valuable discussions. The financial assistance from the Department of Bio-Technology (DBT), the University Grants Commission (UGC) and the Department of Science and Technology (DST), Government of India is gratefully acknowledged.

Appendix A. Supplementary data

Supplementary data associated with this article can be found, in the online version, at doi:10.1016/j.bpc.2006.07.014.

References

[1] H.M. Berman, J. Westbrook, Z. Feng, G. Gilliland, T.N. Bhat, H. Weissig, I.N. Shindyalov, P.E. Bourne, The Protein Data Bank, Nucleic Acids Res. 28 (2000) 235–242.
[2] D.J. Barlow, J.M. Thronton, Helix geometry in proteins, J. Mol. Biol. 201 (1988) 601–619.
[3] S. Kumar, M. Bansal, Structural and sequence characteristics of long alpha helices in globular proteins, Biophys. J. 71 (1996) 1574–1586.
[4] S. Kumar, M. Bansal, Geometrical and sequence characteristics of α-helices in globular proteins, Biophys. J. 75 (1998) 1935–1944.
[5] J.A. Christopher, R. Swanson, T.O. Baldwin, Algorithms for finding the axis of a helix: fast rotational and parametric least-squares methods, Comput. Chem. 20 (1996) 1–21.
[6] M. Bansal, S. Kumar, R. Velavan, HELANAL: a program to characterize helix geometry in proteins, J. Biomol. Struct. Dyn. 17 (2000) 811–819.
[7] S.J. Fleishman, N. Ben-Tal, A novel scoring function for predicting the conformations of tightly packed pairs of transmembrane α-helices, J. Mol. Biol. 321 (2002) 363–378.
[8] R. Srinivasan, S.S. Rajan, Best experimental helical parameters of alpha-helix from protein crystallographic structural data, Curr. Sci. India 46 (1977) 595–596.
[9] R. Srinivasan, R. Balasubramanian, S.S. Rajan, Some new methods and general results of analysis of protein crystallographic structural data, J. Mol. Biol. 98 (1975) 739–747.
[10] R. Balasubramanian, S.S. Rajan, R. Srinivasan, Analysis of protein crystallographic structural data, J. Theor. Biol. 67 (1977) 299–312.
[11] S.S. Rajan, R. Srinivasan, Helical segment analysis of alpha-helical regions in proteins, Biopolymers 16 (1977) 1617–1634.
[12] S.S. Rajan, R. Balasubramanian, R. Srinivasan, Analysis of protein crystallographic structural data: III. Analysis based on segment axes on some proteins, Indian J. Biochem. Biophys. 14 (1977) 14–20.
[13] Y. Goto, L.J. Calciano, A.L. Fink, Acid induced folding of proteins, Proc. Natl. Acad. Sci. U. S. A. 87 (1990) 573–577.
[14] H. Frauenfelder, H. Hartmann, M. Karplus, I.D. Kuntz Jr., L.J. Kuriyan, F. Parak, G.A. Petsko, D. Ringe, R.F. Tilton Jr., M.L. Connolly, N. Max, Thermal expansion of proteins, Biochemistry 26 (1987) 254–261.
[15] G.N. Somero, Proteins and temperature, Annu. Rev. Physiol. 57 (1995) 43–68.
[16] A. Caflisch, M. Karplus, Acid and thermal denaturation of barnase investigated by molecular dynamics simulations, J. Mol. Biol. 252 (1995) 672–708.
[17] G.S. Ratnaparkhi, R. Varadarajan, X-ray crystallographic studies of the denaturation of ribonuclease S, Proteins: Str. Fun. Gen. 36 (1999) 282–294.
[18] A.S. Yang, B. Honig, Structural origins of pH and ionic strength effects on protein stability. Acid denaturation of sperm whale apomyoglobin, J. Mol. Biol. 237 (1994) 602–614.
[19] P.N. Farnsworth, B. Groth-Vasselli, N.J. Greenfield, K. Singh, Effects of temperature and concentration on bovine lens alpha-crystallin secondary structure: a circular dichroism spectroscopic study, Int. J. Biol. Macromol. 20 (1997) 283–291.
[20] M. Zafrullah, Z. Khursheed, S. Yadav, D. Sahgal, S. Jameel, F. Ahmad, Acidic pH enhances structure and structural stability of the capsid protein of hepatitis E virus, Biochem. Biophys. Res. Commun. 313 (2004) 67–73.
[21] M.M. Gromiha, Factors influencing the stability of α-helices and β-strands in thermophilic ribonuclease H, Prep. Biochem. Biotechnol. 31 (2001) 103–112.
[22] K.L. Yap, J.B. Ames, M.B. Swindells, M. Ikura, Vector geometry mapping: a method to characterize the conformation of helix–loop–helix calcium binding proteins, Methods Mol. Biol. 173 (2002) 317–324.
[23] A.C. Drohat, J.C. Amburgey, F. Abildgaard, M.R. Starich, D. Baldisseri, D.J. Weber, Solution structure of rat apo-S100B($^{\beta\beta}$) as determined by NMR spectroscopy, Biochemistry 35 (1996) 11577–11588.
[24] I.V. Kurinov, R.W. Harrison, The influence of temperature on lysozyme crystals. Structure and dynamics of protein and water, Acta Crystallogr., D Biol. Crystallogr. 51 (1995) 98–109.
[25] M.A.T. Blumenschein, T.E. Gillis, G.F. Tibbits, B.D. Sykes, Effect of temperature on the structure of trout troponin C, Biochemistry 43 (2004) 4955–4963.
[26] Y.Z. hang, J. Desharnais, S.E. Greasley, G.P. Beardsley, D.L. Boger, I.A. Wilson, Crystal structures of human GAR Tfase at low and high pH and with substrate $^{\beta}$-GAR, Biochemistry 41 (2002) 14206–14215.
[27] R. Kodandapani, C.G. Suresh, M. Vijayan, Crystal structure of low humidity tetragonal lysozyme at 2.1 Å, J. Biol. Chem. 265 (1990) 16126–16131.
[28] W.J. Cook, L.J. Walter, M.R. Walter, Drug binding by calmodulin: crystal structure of a calmodulin–trifluoperazine complex, Biochemistry 33 (1994) 15259–15265.
[29] A.J. Sharff, L.E. Rodseth, J.C. Spurlino, F.A. Quiocho, Crystallographic evidence of a large ligand-induced hinge–twist motion between the two domains of the maltodextrin binding protein involved in active transport and chemotaxis, Biochemistry 31 (1991) 10657–10663.
[30] P. Briozzo, B. Golinelli-Pimpaneau, A.M. Gilles, J.F. Gaucher, S. Burlacu-Miron, H. Sakamoto, J. Janin, O. Barzu, Structures of *Escherichia coli* CMP kinase alone and in complex with CDP: a new fold of the nucleoside monophosphate binding domain and insights into cytosine nucleotide specificity, Structure 16 (1998) 1517–1527.
[31] A.K.W. Leung, S.D. Henry, F.H. John, M.B. Albert, Crystal structure of the lytic transglycosylase from bacteriophage lambda in complex with hexa-*N*-acetylchitohexaose, Biochemistry 40 (2001) 5665–5673.
[32] J.P. Renaud, N. Rochel, M. Ruff, V. Vivat, P. Chambon, H. Gronemeyer, D. Moras, Crystal structure of the RAR-γ ligand-binding domain bound to all-*trans* retinoic acid, Nature 378 (1995) 681–689.
[33] B.P. Klaholz, A. Mitschler, M. Belema, C. Zusi, D. Moras, Enantiomer discrimination illustrated by high-resolution crystal structures of the human nuclear receptor hRAR-γ, Proc. Natl. Acad. Sci. U. S. A. 97 (2000) 6322–6327.